Applied Mathematics and Mechanics (English Edition), 2007, **28**(5):615–625

Dynamic behavior of two collinear interface cracks between two dissimilar functionally graded piezoelectric/piezomagnetic material strips *

ZHANG Pei-wei (张培伟)[1], ZHOU Zhen-gong (周振功)[1], WANG Biao (王彪)[2]

(1. Center for Composite Materials and Structures, Harbin Institute of Technology, Harbin 150080, P. R. China;

2. School of Physics and Engineering, Sun Yat-Sen University, Guangzhou 510275, P. R. China)

(Contributed by WANG Biao)

Abstract The dynamic interaction of two collinear interface cracks between two dissimilar functionally graded piezoelectric/piezomagnetic material strips subjected to the anti-plane shear harmonic stress waves was investigated. By using the Fourier transform, the problem can be solved with the help of a pair of triple integral equations in which the unknown variable is jump of displacement across the crack surfaces. These equations are solved using the Schmidt method. Numerical examples are provided to show the effect of the functionally graded parameter, the circular frequency of the incident waves and the thickness of the strip upon stress, electric displacement and magnetic flux intensity factors of cracks.

Key words functionally graded piezoelectric/piezomagnetic materials, interface crack, stress wave

Chinese Library Classification O345.41
2000 Mathematics Subject Classification 74J20, 74R10, 74F15
Digital Object Identifier(DOI) 10.1007/s 10483-007-0507-1

Introduction

With increasingly wide application of piezoelectric/piezomagnetic composites in smart material systems, cavity or crack problems in magnetoelectroelastic media have received considerable interest[1−3]. Some application of functionally graded piezoelectric materials have been made[4]. The fracture problems of functionally graded piezoelectric materials have been considered in Refs.[5,6]. Li and Weng[6] first considered the static anti-plane problem of a finite crack in functionally graded piezoelectric material strip.

Recently, the fracture problems of functionally graded piezoelectric/piezomagnetic materials have been firstly considered in Refs.[7,8]. The concept of functionally graded materials was also extended to the piezoelectric/piezomagnetic materials to study the fracture behaviors of piezoelectric/piezomagnetic materials and structures. However, only the static anti-plane shear fracture problems in unbounded media were considered in Refs.[7,8]. The fracture mechanics in piezoelectric/piezomagnetic composites[7,8] deals with unbounded media and, therefore, is not suitable for materials characterization. Simultaneously, relatively few works have been made for the dynamic behavior of cracks in functionally graded piezoelectric/piezomagnetic materials. To our knowledge, the magneto-electro-elastic dynamic behavior of two collinear interface cracks

* Received Nov.20, 2006; Revised Jan.25, 2007
Project supported by the National Natural Science Foundation of China (Nos.10572043,10572155) and the Natural Science Foundation with Excellent Young Investigators of Heilongjiang Province (No.JC04-08)
Corresponding author ZHANG Pei-wei, Doctor, E-mail:zhouzhg@hit.edu.cn

between two dissimilar functionally graded piezoelectric/piezomagnetic material strips of finite thickness has not been studied by using Schmidt method[9].

In this paper, we attempt to extend the concept of functionally graded materials to study the dynamic fracture behaviors of piezoelectric/piezomagnetic materials. The magneto-electro-elastic dynamic behavior of two collinear interface cracks between two dissimilar functionally graded piezoelectric/piezomagnetic material strip subjected to the harmonic anti-plane shear stress waves was investigated using Schmidt method[9]. To make the analysis tractable, it was assumed that the material properties vary exponentially with coordinate vertical to the crack. Fourier transform was applied and a mixed boundary value problem is reduced to a pair of triple integral equations. To solve the triple integral equations, the jump of displacements across crack surfaces was directly expanded in a series of Jacobi polynomials. Numerical examples are provided to show the effect of the functionally graded parameter, the circular frequency of the incident waves and the thickness of the strip upon stress, electric displacement and magnetic flux intensity factors of cracks.

1 Formulation of problem

It is assumed that there are two collinear interface cracks with length of $1-b$ between two dissimilar functionally graded piezoelectric/piezomagnetic material strips as shown in Fig.1. $2b$ is the distance between the two cracks (The solution of two collinear cracks of length $d-b$ in functionally graded piezoelectric/piezomagnetic materials can easily be obtained by a simple change in the numerical values of the present paper for crack length of $1-b/d$, $d>b>0$). h_1 and h_2 are the thickness of the upper and the lower functionally graded piezoelectric/piezomagnetic material strip, respectively. In the present paper, b, h_1 and h_2 are all non-dimensional variables. It is also assumed that the propagation direction of the anti-plane shear harmonic stress wave is vertical to the crack. Let ω be the circular frequency of the incident wave. $w_0^{(i)}(x,y,t), \phi_0^{(i)}(x,y,t)$ and $\psi_0^{(i)}(x,y,t)(i=1,2)$are mechanical displacement, electric potential and magnetic potential, respectively. $\tau_{zk0}^{(i)}(x,y,t)$, $D_{k0}^{(i)}(x,y,t)$ and $B_{k0}^{(i)}(x,y,t)$ $(k=x,y;\ i=1,2)$ are anti-plane shear stress field, in-plane electric displacement field and in-plane magnetic flux, respectively. Also note that all quantities with superscript $i(i=1,2)$ refer to the upper layer 1 and the lower layer 2 as shown in Fig.1, respectively. Because the incident waves are the harmonic anti-plane shear stress waves, all field quantities of $w_0^{(i)}(x,y,t), \phi_0^{(i)}(x,y,t), \psi_0^{(i)}(x,y,t)$, $\tau_{zk0}^{(i)}(x,y,t)$, $D_{k0}^{(i)}(x,y,t)$ and $B_{k0}^{(i)}(x,y,t)$ can be assumed to be of the forms as follows:

$$
\begin{aligned}
&[w_0^{(i)}(x,y,t), \phi_0^{(i)}(x,y,t), \psi_0^{(i)}(x,y,t), \tau_{zk0}^{(i)}(x,y,t), D_{k0}^{(i)}(x,y,t), B_{k0}^{(i)}(x,y,t)] \\
&= [w^{(i)}(x,y), \phi^{(i)}(x,y), \psi^{(i)}(x,y), \tau_{zk}^{(i)}(x,y), D_k^{(i)}(x,y), B_k^{(i)}(x,y)]\mathrm{e}^{-\mathrm{i}\omega t}. \qquad (1)
\end{aligned}
$$

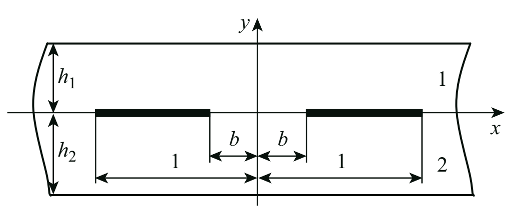

Fig.1 Geometry and coordinate system for two collinear interface cracks

In what follows, the time dependence of $\mathrm{e}^{-\mathrm{i}\omega t}$ will be suppressed for brevity. As discussed in Ref.[10], permeable condition will be enforced in the present study. Here, the standard superposition technique is used and only the perturbation fields are considered in the present paper. So the boundary conditions of the present problem can be written as follows:

$$\begin{cases}\tau_{yz}^{(1)}(x,0^+)=\tau_{yz}^{(2)}(x,0^-)=-\tau_0, & b\le|x|\le 1,\\ \tau_{yz}^{(1)}(x,0^+)=\tau_{yz}^{(2)}(x,0^-),\quad w^{(1)}(x,0^+)=w^{(2)}(x,0^-), & |x|>1,|x|<b;\end{cases}\tag{2}$$

$$\begin{cases}\phi^{(1)}(x,0)=\phi^{(2)}(x,0), D_y^{(1)}(x,0)=D_y^{(2)}(x,0),\\ \psi^{(1)}(x,0)=\psi^{(2)}(x,0), B_y^{(1)}(x,0)=B_y^{(2)}(x,0),\end{cases}\quad |x|<\infty;\tag{3}$$

$$\begin{cases}\tau_{yz}^{(1)}(x,h_1)=\tau_{yz}^{(2)}(x,-h_2)=0,\\ D_y^{(1)}(x,h_1)=D_y^{(2)}(x,-h_2)=0,\\ B_y^{(1)}(x,h_1)=B_y^{(2)}(x,-h_2)=0,\end{cases}\quad |x|<\infty;\tag{4}$$

$$\begin{cases}w^{(1)}(x,y)=w^{(2)}(x,y)=0,\\ \phi^{(1)}(x,y)=\phi^{(2)}(x,y)=0,\\ \psi^{(1)}(x,y)=\psi^{(2)}(x,y)=0,\end{cases}\quad (x^2+y^2)^{1/2}\to\infty.\tag{5}$$

In this paper, τ_0 is the magnitude of the anti-plane shear harmonic waves.

Crack problems in functionally graded piezoelectric/piezomagnetic materials do not appear to be analytically tractable for arbitrary variations of material properties. Usually, one tries to generate the forms of non-homogeneities for which the problem becomes tractable. Similar to the treatment of the crack problem for isotropic functionally graded materials in Ref.[11], we assume the material properties are described by

$$\begin{cases}c_{44}^{(1)}=c_{440}^{(1)}\mathrm{e}^{\beta^{(1)}y},\quad e_{15}^{(1)}=e_{150}^{(1)}\mathrm{e}^{\beta^{(1)}y},\quad \varepsilon_{11}^{(1)}=\varepsilon_{110}^{(1)}\mathrm{e}^{\beta^{(1)}y},\\ q_{15}^{(1)}=q_{150}^{(1)}\mathrm{e}^{\beta^{(1)}y},\quad d_{11}^{(1)}=d_{110}^{(1)}\mathrm{e}^{\beta^{(1)}y},\quad \mu_{11}^{(1)}=\mu_{110}^{(1)}\mathrm{e}^{\beta^{(1)}y},\quad \rho^{(1)}(y)=\rho_0^{(1)}\mathrm{e}^{\beta^{(1)}y},\\ c_{44}^{(2)}=c_{440}^{(2)}\mathrm{e}^{\beta^{(2)}y},\quad e_{15}^{(2)}=e_{150}^{(2)}\mathrm{e}^{\beta^{(2)}y},\quad \varepsilon_{11}^{(2)}=\varepsilon_{110}^{(2)}\mathrm{e}^{\beta^{(2)}y},\\ q_{15}^{(2)}=q_{150}^{(2)}\mathrm{e}^{\beta^{(2)}y},\quad d_{11}^{(2)}=d_{110}^{(2)}\mathrm{e}^{\beta^{(2)}y},\quad \mu_{11}^{(2)}=\mu_{110}^{(2)}\mathrm{e}^{\beta^{(2)}y},\quad \rho^{(2)}(y)=\rho_0^{(2)}\mathrm{e}^{\beta^{(2)}y},\end{cases}\tag{6}$$

where $c_{440}^{(i)}, e_{150}^{(i)}, \varepsilon_{110}^{(i)}, q_{150}^{(i)}, d_{110}^{(i)}, \mu_{110}^{(i)}$ and $\beta^{(i)}$ are the shear modulus, the piezoelectric coefficient, the dielectric parameter, the piezomagnetic coefficient, the magnetoelectric coefficient, the magnetic permeability and the functionally graded parameter of two dissimilar functionally graded piezoelectric/piezomagnetic material strips, respectively.

The constitutive equations for the mode III crack can be expressed as follows:

$$\begin{cases}\tau_{zk}^{(i)}=c_{44}^{(i)}w_{,k}^{(i)}+e_{15}^{(i)}\phi_{,k}^{(i)}+q_{15}^{(i)}\psi_{,k}^{(i)},\\ D_k^{(i)}=e_{15}^{(i)}w_{,k}^{(i)}-\varepsilon_{11}^{(i)}\phi_{,k}^{(i)}-d_{11}^{(i)}\psi_{,k}^{(i)},\\ B_k^{(i)}=q_{15}^{(i)}w_{,k}^{(i)}-d_{11}^{(i)}\phi_{,k}^{(i)}-\mu_{11}^{(i)}\psi_{,k}^{(i)},\end{cases}\quad k=x,y;\quad i=1,2.\tag{7}$$

The anti-plane governing equations are

$$\begin{cases}c_{440}^{(i)}(\nabla^2w^{(i)}+\beta^{(i)}\dfrac{\partial w^{(i)}}{\partial y})+e_{150}^{(i)}(\nabla^2\phi^{(i)}+\beta^{(i)}\dfrac{\partial\phi^{(i)}}{\partial y})+q_{150}^{(i)}(\nabla^2\psi^{(i)}+\beta^{(i)}\dfrac{\partial\psi^{(i)}}{\partial y})=-\rho_0^{(i)}\omega^2w^{(i)},\\ e_{150}^{(i)}(\nabla^2w^{(i)}+\beta^{(i)}\dfrac{\partial w^{(i)}}{\partial y})-\varepsilon_{110}^{(i)}(\nabla^2\phi^{(i)}+\beta^{(i)}\dfrac{\partial\phi^{(i)}}{\partial y})-d_{110}^{(i)}(\nabla^2\psi^{(i)}+\beta^{(i)}\dfrac{\partial\psi^{(i)}}{\partial y})=0,\\ q_{150}^{(i)}(\nabla^2w^{(i)}+\beta^{(i)}\dfrac{\partial w^{(i)}}{\partial y})-d_{110}^{(i)}(\nabla^2\phi^{(i)}+\beta^{(i)}\dfrac{\partial\phi^{(i)}}{\partial y})-\mu_{110}^{(i)}(\nabla^2\psi^{(i)}+\beta^{(i)}\dfrac{\partial\psi^{(i)}}{\partial y})=0,\end{cases}\tag{8}$$

where $-\rho_0^{(i)}\omega^2w^{(i)}(x,y)\mathrm{e}^{-\mathrm{i}\omega t}=\rho_0^{(i)}\frac{\partial^2w_0^{(i)}(x,y,t)}{\partial t^2}=\rho_0^{(i)}\frac{\partial^2(w^{(i)}(x,y)\mathrm{e}^{-\mathrm{i}\omega t})}{\partial t^2}$. $\nabla^2=\frac{\partial^2}{\partial x^2}+\frac{\partial^2}{\partial y^2}$ is the two dimensional Laplace operator.

2 Solutions

Because of the assumed symmetry in geometry and loading, it is sufficient to consider the problem for $0 \le x < \infty, -h_2 \le y < h_1$ only. The system of above governing equation (8) is solved using the Fourier integral transform. The general expressions for displacement components, electric potentials and magnetic potentials can be written, respectively, as follows:

$$\begin{cases} w^{(1)}(x,y) = \dfrac{2}{\pi}\displaystyle\int_0^\infty [A_1(s)\mathrm{e}^{-\gamma_1^{(1)}y} + B_1(s)\mathrm{e}^{\gamma_1^{(1)}y}]\cos(sx)ds, \\ \phi^{(1)}(x,y) = a_0^{(1)}w^{(1)}(x,y) + \dfrac{2}{\pi}\displaystyle\int_0^\infty [C_1(s)\mathrm{e}^{-\gamma_2^{(1)}y} + D_1(s)\mathrm{e}^{\gamma_2^{(1)}y}]\cos(sx)ds, \\ \psi^{(1)}(x,y) = a_1^{(1)}w^{(1)}(x,y) + \dfrac{2}{\pi}\displaystyle\int_0^\infty [E_1(s)\mathrm{e}^{-\gamma_2^{(1)}y} + F_1(s)\mathrm{e}^{\gamma_2^{(1)}y}]\cos(sx)ds; \end{cases} \tag{9}$$

$$\begin{cases} w^{(2)}(x,y) = \dfrac{2}{\pi}\displaystyle\int_0^\infty [A_2(s)\mathrm{e}^{\gamma_1^{(2)}y} + B_2(s)\mathrm{e}^{-\gamma_1^{(2)}y}]\cos(sx)ds, \\ \phi^{(2)}(x,y) = a_0^{(2)}w^{(2)}(x,y) + \dfrac{2}{\pi}\displaystyle\int_0^\infty [C_2(s)\mathrm{e}^{\gamma_2^{(2)}y} + D_2(s)\mathrm{e}^{-\gamma_2^{(2)}y}]\cos(sx)ds, \\ \psi^{(2)}(x,y) = a_1^{(2)}w^{(2)}(x,y) + \dfrac{2}{\pi}\displaystyle\int_0^\infty [E_2(s)\mathrm{e}^{\gamma_2^{(2)}y} + F_2(s)\mathrm{e}^{-\gamma_2^{(2)}y}]\cos(sx)ds, \end{cases} \tag{10}$$

where $A_i, B_i, C_i, D_i, E_i, F_i (i = 1, 2)$ are unknown functions. $\gamma_1^{(1)} = (\beta^{(1)} + \sqrt{\beta^{(1)2} + 4[s^2 - \omega^2/c_1^2]})/2$, $\gamma_2^{(1)} = (\beta^{(1)} + \sqrt{\beta^{(1)2} + 4s^2})/2$, $c_1 = \sqrt{\mu_0^{(1)}/\rho_0^{(1)}}$ is the shear wave velocity of the upper layer material. $\mu_0^{(1)} = c_{440}^{(1)} + a_0^{(1)}e_{150}^{(1)} + a_1^{(1)}q_{150}^{(1)}$, $a_0^{(1)} = (\mu_{110}^{(1)}e_{150}^{(1)} - d_{110}^{(1)}q_{150}^{(1)})/(\varepsilon_{110}^{(1)}\mu_{110}^{(1)} - d_{110}^{(1)2})$, $a_1^{(1)} = (q_{150}^{(1)}\varepsilon_{110}^{(1)} - d_{110}^{(1)}e_{150}^{(1)})/(\varepsilon_{110}^{(1)}\mu_{110}^{(1)} - d_{110}^{(1)2})$, $\gamma_1^{(2)} = (\beta^{(2)} + \sqrt{\beta^{(2)2} + 4[s^2 - \omega^2/c_2^2]})/2$, $\gamma_2^{(2)} = (\beta^{(2)} + \sqrt{\beta^{(2)2} + 4s^2})/2$, $c_2 = \sqrt{\mu_0^{(2)}/\rho_0^{(2)}}$ is the shear wave velocity of the lower layer material. $\mu_0^{(2)} = c_{440}^{(2)} + a_0^{(2)}e_{150}^{(2)} + a_1^{(2)}q_{150}^{(2)}$, $a_0^{(2)} = (\mu_{110}^{(2)}e_{150}^{(2)} - d_{110}^{(2)}q_{150}^{(2)})/(\varepsilon_{110}^{(2)}\mu_{110}^{(2)} - d_{110}^{(2)2})$, $a_1^{(2)} = (q_{150}^{(2)}\varepsilon_{110}^{(2)} - d_{110}^{(2)}e_{150}^{(2)})/(\varepsilon_{110}^{(2)}\mu_{110}^{(2)} - d_{110}^{(2)2})$.

So from Eq.(7), we have

$$\begin{aligned} \tau_{yz}^{(1)}(x,y) = &-\frac{2\mathrm{e}^{\beta^{(1)}y}}{\pi}\int_0^\infty \{\mu_0^{(1)}\gamma_1^{(1)}[A_1(s)\mathrm{e}^{-\gamma_1^{(1)}y} - B_1(s)\mathrm{e}^{\gamma_1^{(1)}y}] \\ &+ e_{150}^{(1)}\gamma_2^{(1)}[C_1(s)\mathrm{e}^{-\gamma_1^{(2)}y} - D_1(s)\mathrm{e}^{\gamma_1^{(2)}y}] \\ &+ q_{150}^{(1)}\gamma_2^{(1)}[E_1(s)\mathrm{e}^{-\gamma_2^{(1)}y} - F_1(s)\mathrm{e}^{\gamma_2^{(1)}y}]\}\cos(sx)ds, \end{aligned} \tag{11}$$

$$\begin{aligned} D_y^{(1)}(x,y) = &\frac{2\mathrm{e}^{\beta^{(1)}y}}{\pi}\int_0^\infty \gamma_2^{(1)}\{\varepsilon_{110}^{(1)}[C_1(s)\mathrm{e}^{-\gamma_2^{(1)}y} - D_1(s)\mathrm{e}^{\gamma_2^{(1)}y}] \\ &+ d_{110}^{(1)}[E_1(s)\mathrm{e}^{-\gamma_2^{(1)}y} - F_1(s)\mathrm{e}^{\gamma_2^{(1)}y}]\}\cos(sx)ds, \end{aligned} \tag{12}$$

$$\begin{aligned} B_y^{(1)}(x,y) = &\frac{2\mathrm{e}^{\beta^{(1)}y}}{\pi}\int_0^\infty \gamma_2^{(1)}\{d_{110}^{(1)}[C_1(s)\mathrm{e}^{-\gamma_2^{(1)}y} - D_1(s)\mathrm{e}^{\gamma_2^{(1)}y}] \\ &+ \mu_{110}^{(1)}[E_1(s)\mathrm{e}^{-\gamma_2^{(1)}y} - F_1(s)\mathrm{e}^{\gamma_2^{(1)}y}]\}\cos(sx)ds, \end{aligned} \tag{13}$$

$$\begin{aligned} \tau_{yz}^{(2)}(x,y) = &\frac{2\mathrm{e}^{\beta^{(2)}y}}{\pi}\int_0^\infty \{\mu_0^{(2)}\gamma_1^{(2)}[A_2(s)\mathrm{e}^{\gamma_1^{(2)}y} - B_2(s)\mathrm{e}^{-\gamma_1^{(2)}y}] \\ &+ e_{150}^{(2)}\gamma_2^{(2)}[C_2(s)\mathrm{e}^{\gamma_2^{(2)}y} - D_2(s)\mathrm{e}^{-\gamma_2^{(2)}y}] \end{aligned}$$

$$+ q_{150}^{(2)}[E_2(s)\mathrm{e}^{\gamma_2^{(2)}y} - F_2(s)\mathrm{e}^{-\gamma_2^{(2)}y}]\}\cos(sx)ds, \tag{14}$$

$$D_y^{(2)}(x,y) = -\frac{2\mathrm{e}^{\beta^{(2)}y}}{\pi}\int_0^\infty \gamma_2^{(2)}\{\varepsilon_{110}^{(2)}[C_2(s)\mathrm{e}^{\gamma_2^{(2)}y} - D_2(s)\mathrm{e}^{-\gamma_2^{(2)}y}] + d_{110}^{(2)}[E_2(s)\mathrm{e}^{\gamma_2^{(2)}y} - F_2(s)\mathrm{e}^{-\gamma_2^{(2)}y}]\}\cos(sx)ds, \tag{15}$$

$$B_y^{(2)}(x,y) = -\frac{2\mathrm{e}^{\beta^{(2)}y}}{\pi}\int_0^\infty \gamma_2^{(2)}\{d_{110}^{(2)}[C_2(s)\mathrm{e}^{\gamma_2^{(2)}y} - D_2(s)\mathrm{e}^{-\gamma_2^{(2)}y}] + \mu_{110}^{(2)}[E_2(s)\mathrm{e}^{\gamma_2^{(2)}y} - F_2(s)\mathrm{e}^{-\gamma_2^{(2)}y}]\}\cos(sx)ds. \tag{16}$$

To solve the problem, the jump of displacements across crack surfaces is defined as

$$f(x) = w^{(1)}(x,0) - w^{(2)}(x,0). \tag{17}$$

Substituting Eqs.(9)–(10) into Eqs.(17), and applying the Fourier transform and the boundary conditions (2)–(4), it can be given

$$A_1(s) + B_1(s) - A_2(s) - B_2(s) = \bar{f}(s), \tag{18}$$

$$a_0^{(1)}[A_1(s) + B_1(s)] - a_0^{(2)}[A_2(s) + B_2(s)] + C_1(s) + D_1(s) - C_2(s) - D_2(s) = 0, \tag{19}$$

$$a_1^{(1)}[A_1(s) + B_1(s)] - a_1^{(2)}[A_2(s) + B_2(s)] + E_1(s) + F_1(s) - E_2(s) - F_2(s) = 0, \tag{20}$$

$$\mu_0^{(1)}\gamma_1^{(1)}[A_1(s)\mathrm{e}^{-\gamma_1^{(1)}h_1} - B_1(s)\mathrm{e}^{\gamma_1^{(1)}h_1}] + e_{150}^{(1)}\gamma_2^{(1)}[C_1(s)\mathrm{e}^{-\gamma_2^{(1)}h_1} - D_1(s)\mathrm{e}^{\gamma_2^{(1)}h_1}] + q_{150}^{(1)}\gamma_2^{(1)}[E_1(s)\mathrm{e}^{-\gamma_2^{(1)}h_1} - F_1(s)\mathrm{e}^{\gamma_2^{(1)}h_1}] = 0, \tag{21}$$

$$\varepsilon_{110}^{(1)}[C_1(s)\mathrm{e}^{-\gamma_2^{(1)}h_1} - D_1(s)\mathrm{e}^{\gamma_2^{(1)}h_1}] + d_{110}^{(1)}[E_1(s)\mathrm{e}^{-\gamma_2^{(1)}h_1} - F_1(s)\mathrm{e}^{\gamma_2^{(1)}h_1}] = 0, \tag{22}$$

$$d_{110}^{(1)}[C_1(s)\mathrm{e}^{-\gamma_2^{(1)}h_1} - D_1(s)\mathrm{e}^{\gamma_2^{(1)}h_1}] + \mu_{110}^{(1)}[E_1(s)\mathrm{e}^{-\gamma_2^{(1)}h_1} - F_1(s)\mathrm{e}^{\gamma_2^{(1)}h_1}] = 0, \tag{23}$$

$$\mu_0^{(2)}\gamma_1^{(2)}[A_2(s)\mathrm{e}^{-\gamma_1^{(2)}h_2} - B_2(s)\mathrm{e}^{\gamma_1^{(2)}h_2}] + e_{150}^{(2)}\gamma_2^{(2)}[C_2(s)\mathrm{e}^{-\gamma_2^{(2)}h_2} - D_2(s)\mathrm{e}^{\gamma_2^{(2)}h_2}] + q_{150}^{(2)}[E_2(s)\mathrm{e}^{-\gamma_2^{(2)}h_2} - F_2(s)\mathrm{e}^{\gamma_2^{(2)}h_2}] = 0, \tag{24}$$

$$\varepsilon_{110}^{(2)}[C_2(s)\mathrm{e}^{-\gamma_2^{(2)}h_2} - D_2(s)\mathrm{e}^{\gamma_2^{(2)}h_2}] + d_{110}^{(2)}[E_2(s)\mathrm{e}^{-\gamma_2^{(2)}h_2} - F_2(s)\mathrm{e}^{\gamma_2^{(2)}h_2}] = 0, \tag{25}$$

$$d_{110}^{(2)}[C_2(s)\mathrm{e}^{-\gamma_2^{(2)}h_2} - D_2(s)\mathrm{e}^{\gamma_2^{(2)}h_2}] + \mu_{110}^{(2)}[E_2(s)\mathrm{e}^{-\gamma_2^{(2)}h_2} - F_2(s)\mathrm{e}^{\gamma_2^{(2)}h_2}] = 0. \tag{26}$$

A superposed bar indicates the Fourier transform throughout this paper. Substituting Eqs.(11)–(16) into Eqs.(2)–(3), we have

$$\{\mu_0^{(1)}\gamma_1^{(1)}[A_1(s) - B_1(s)] + \gamma_2^{(1)}e_{150}^{(1)}[C_1(s) - D_1(s)] + q_{150}^{(1)}\gamma_2^{(1)}[E_1(s) - F_1(s)]\} + \{\mu_0^{(2)}\gamma_1^{(2)}[A_2(s) - B_2(s)] + e_{150}^{(2)}\gamma_2^{(2)}[C_2(s) - D_2(s)] + q_{150}^{(2)}\gamma_2^{(2)}[E_2(s) - F_2(s)]\} = 0, \tag{27}$$

$$\gamma_2^{(1)}\{\varepsilon_{110}^{(1)}[C_1(s) - D_1(s)] + d_{110}^{(1)}[E_1(s) - F_1(s)]\} + \gamma_2^{(2)}\{\varepsilon_{110}^{(2)}[C_2(s) - D_2(s)] + d_{110}^{(2)}[E_2(s) - F_2(s)]\} = 0, \tag{28}$$

$$\gamma_2^{(1)}\{d_{110}^{(1)}[C_1(s) - D_1(s)] + \mu_{110}^{(1)}[E_1(s) - F_1(s)]\} + \gamma_2^{(2)}\{d_{110}^{(2)}[C_2(s) - D_2(s)] + \mu_{110}^{(2)}[E_2(s) - F_2(s)]\} = 0. \tag{29}$$

By solving twelve equations (18)–(29) with twelve unknown functions $A_i, B_i, C_i, D_i, E_i, F_i (i = 1, 2)$ and applying the boundary conditions (2)–(3), it can be obtained that

$$\frac{2}{\pi}\int_0^\infty \bar{f}(s)\cos(sx)ds = 0, \quad x > 1, 0 < x < b, \tag{30}$$

$$\frac{2}{\pi}\int_0^\infty g_1(s)\bar{f}(s)\cos(sx)ds = -\tau_0, \quad b \le x \le 1, \tag{31}$$

where $g_1(s)$ is a known function of the variable s, the thickness of the strip and the material properties. Here the expression of $g_1(s)$ was omitted for brevity. $\lim_{s\to\infty} g_1(s)/s = \alpha_1$. α_1 is a constant which depends on the properties of the materials. However, α_1 is independent of the functionally graded parameters $\beta^{(1)}$ and $\beta^{(2)}$. Here the expression of α_1 was also omitted for brevity. It can be obtained that $\alpha_1 = -c_{440}^{(1)}/2$ for $(c_{440}^{(1)}, e_{150}^{(1)}, \varepsilon_{110}^{(1)}, q_{150}^{(1)}, d_{110}^{(1)}, \mu_{110}^{(1)}, \rho_0^{(1)}) = (c_{440}^{(2)}, e_{150}^{(2)}, \varepsilon_{110}^{(2)}, q_{150}^{(2)}, d_{110}^{(2)}, \mu_{110}^{(2)}, \rho_0^{(2)})$. To determine the unknown function $\bar{f}(s)$, the above triple integral equations (30)–(31) must be solved.

3 Solution of triple integral equations

The Schmidt method[9] is used to solve the triple integral equations (30)–(31). The jump of displacement across crack surfaces is represented by the following series:

$$f(x) = \sum_{n=0}^{\infty} b_n P_n^{(\frac{1}{2},\frac{1}{2})}\left(\frac{x - \frac{1+b}{2}}{\frac{1-b}{2}}\right)\left(1 - \frac{(x - \frac{1+b}{2})^2}{(\frac{1-b}{2})^2}\right)^{\frac{1}{2}}, \quad b \le x \le 1, \tag{32}$$

$$f(x) = w^{(1)}(x,0) - w^{(2)}(x,0) = 0, \quad x > 1,\ 0 < x < b, \tag{33}$$

where b_n are unknown coefficients to be determined and $P_n^{(1/2,1/2)}(x)$ is a Jacobi polynomial[12]. The Fourier transform of Eqs.(32)–(33) is[13]

$$\bar{f}(s) = \sum_{n=0}^{\infty} b_n F_n G_n(s) \frac{1}{s} \mathrm{J}_{n+1}\left(s\frac{1-b}{2}\right), \tag{34}$$

where $F_n = 2\sqrt{\pi}\frac{\Gamma(n+1+1/2)}{n!}$, $G_n(s) = \begin{cases} (-1)^{\frac{n}{2}}\cos(s\frac{1+b}{2}), n = 0, 2, 4, \cdots \\ (-1)^{\frac{n+1}{2}}\sin(s\frac{1+b}{2}), n = 1, 3, 5, \cdots \end{cases}$. $\Gamma(x)$ and $\mathrm{J}_n(x)$ are the Gamma and Bessel functions, respectively.

Substituting Eq.(34) into Eqs.(30)–(31), respectively, it can be shown that Eq.(30) is automatically satisfied. After integration with respect to x in $[b, x]$, Eq.(31) reduces to

$$\frac{2}{\pi}\sum_{n=0}^{\infty} b_n F_n \int_0^\infty \frac{1}{s^2} g_1(s) G_n(s) \mathrm{J}_{n+1}\left(s\frac{1-b}{2}\right)[\sin(sx) - \sin(sb)]ds = -\tau_0(x - b), \quad b \le x \le 1. \tag{35}$$

Equation (35) can now be solved for the coefficients b_n by the Schmidt method[9]. For details, please see Refs.[14]–[17].

4 Intensity factors

The coefficients b_n are known, so that the entire perturbation stress, electric displacement and magnetic flux fields can be obtained. However, in fracture mechanics, it is of importance to determine perturbation stress, perturbation electric displacement and perturbation magnetic flux in the vicinity of crack tips. In the case of the present study,$\tau_{yz}^{(1)}$,$D_y^{(1)}$ and $B_y^{(1)}$ along the crack line can be expressed, respectively, as

$$\tau_{yz}^{(1)}(x,0)=\tau_{yz}^{(2)}(x,0)=\frac{2}{\pi}\sum_{n=0}^{\infty}b_nF_n\int_0^{\infty}\frac{1}{s}g_1(s)G_n(s)\mathrm{J}_{n+1}\left(s\frac{1-b}{2}\right)\cos(xs)ds, \tag{36}$$

$$D_y^{(1)}(x,0)=D_y^{(2)}(x,0)=\frac{2}{\pi}\sum_{n=0}^{\infty}b_nF_n\int_0^{\infty}\frac{1}{s}g_2(s)G_n(s)\mathrm{J}_{n+1}\left(s\frac{1-b}{2}\right)\cos(xs)ds, \tag{37}$$

$$B_y^{(1)}(x,0)=B_y^{(2)}(x,0)=\frac{2}{\pi}\sum_{n=0}^{\infty}b_nF_n\int_0^{\infty}\frac{1}{s}g_3(s)G_n(s)\mathrm{J}_{n+1}\left(s\frac{1-b}{2}\right)\cos(xs)ds, \tag{38}$$

where $g_2(s)$ and $g_3(s)$ are known functions of the variable s, the thickness of the strip and the material properties. The expressions of $g_2(s)$ and $g_3(s)$ were omitted for brevity. $\lim\limits_{s\to\infty}g_2(s)/s=\alpha_2$, $\lim\limits_{s\to\infty}g_3(s)/s=\alpha_3$, where α_2 and α_3 are two constants which depend on the properties of the materials. The expressions of α_2 and α_3 were also omitted for brevity. It can be obtained that $\alpha_2=-e_{150}^{(1)}/2$ and $\alpha_3=-q_{150}^{(1)}/2$ for $(c_{440}^{(1)},e_{150}^{(1)},\varepsilon_{110}^{(1)},q_{150}^{(1)},d_{110}^{(1)},\mu_{110}^{(1)},\rho_0^{(1)})=(c_{440}^{(2)},e_{150}^{(2)},\varepsilon_{110}^{(2)},q_{150}^{(2)},d_{110}^{(2)},\mu_{110}^{(2)},\rho_0^{(2)})$.

The singular parts of stress field, electric displacement and magnetic flux near crack tips in Eqs.(36)–(38) can be expressed respectively as ($x>1$ or $x<b$)

$$\tau=\frac{\alpha_1}{\pi}\sum_{n=0}^{\infty}b_nF_nH_n(b,x),\quad D=\frac{\alpha_2}{\pi}\sum_{n=0}^{\infty}b_nF_nH_n(b,x),\quad B=\frac{\alpha_3}{\pi}\sum_{n=0}^{\infty}b_nF_nH_n(b,x), \tag{39}$$

where

$$H_n(b,x)=\begin{cases}(-1)^{n+1}R(b,x,n), & 0<x<b,\\ -R(b,x,n), & x>1,\end{cases}$$

$$R(b,x,n)=\frac{2(1-b)^{n+1}}{\sqrt{|1+b-2x|^2-(1-b)^2}[|1+b-2x|+\sqrt{|1+b-2x|^2-(1-b)^2}]^{n+1}}.$$

The stress intensity factors K_{L}, electric displacement intensity factors K_{L}^D and magnetic flux intensity factors K_{L}^B at the left tip of the right crack can be expressed respectively as

$$K_{\mathrm{L}}=\lim_{x\to b^-}\sqrt{2(b-x)}\cdot\tau=-\frac{\alpha_1}{\pi}\sqrt{\frac{2}{(1-b)}}\sum_{n=0}^{\infty}(-1)^nb_nF_n, \tag{40}$$

$$K_{\mathrm{L}}^D=\lim_{x\to b^-}\sqrt{2(b-x)}\cdot D=-\frac{\alpha_2}{\pi}\sqrt{\frac{2}{(1-b)}}\sum_{n=0}^{\infty}(-1)^nb_nF_n=\frac{\alpha_2}{\alpha_1}K_{\mathrm{L}}, \tag{41}$$

$$K_{\mathrm{L}}^B=\lim_{x\to b^-}\sqrt{2(b-x)}\cdot B=-\frac{\alpha_3}{\pi}\sqrt{\frac{2}{(1-b)}}\sum_{n=0}^{\infty}(-1)^nb_nF_n=\frac{\alpha_3}{\alpha_1}K_{\mathrm{L}}. \tag{42}$$

The stress intensity factors K_{R}, electric displacement intensity factors K_{R}^D and magnetic flux intensity factors K_{R}^B at the right tip of the right crack can be expressed respectively as

$$K_{\mathrm{R}}=\lim_{x\to 1^+}\sqrt{2(x-1)}\cdot\tau=-\frac{\alpha_1}{\pi}\sqrt{\frac{2}{(1-b)}}\sum_{n=0}^{\infty}b_nF_n, \tag{43}$$

$$K_{\mathrm{R}}^D=\lim_{x\to 1^+}\sqrt{2(x-1)}\cdot D=-\frac{\alpha_2}{\pi}\sqrt{\frac{2}{(1-b)}}\sum_{n=0}^{\infty}b_nF_n=\frac{\alpha_2}{\alpha_1}K_{\mathrm{R}}, \tag{44}$$

$$K_{\mathrm{R}}^{B} = \lim_{x \to 1^{+}} \sqrt{2(x-1)} \cdot B = -\frac{\alpha_3}{\pi} \sqrt{\frac{2}{(1-b)}} \sum_{n=0}^{\infty} b_n F_n = \frac{\alpha_3}{\alpha_1} K_{\mathrm{R}}. \tag{45}$$

5 Numerical calculations and discussion

As discussed in Refs.[16,17], it can be seen that the Schmidt method performs satisfactorily if the first ten terms of the infinite series in Eq.(35) are retained. In all computations, according to Ref.[1], the constants of materials-I are assumed to be that $c_{440}^{(1)} = 44.0$ GPa, $e_{150}^{(1)} = 5.8$ C/m^2, $\varepsilon_{110}^{(1)} = 5.64 \times 10^{-9}$ C^2 /(N·m^2), $q_{150}^{(1)} = 275.0$ N/(A·m), $d_{110}^{(1)} = 0.005 \times 10^{-9}$ N·s/(V·C), $\mu_{110}^{(1)} = -297.0 \times 10^{-6}$ N·s^2 /C^2, $\rho_0^{(1)} = 1\,500$ kg/m^3 and the constants of materials-II are assumed to be that $c_{440}^{(2)} = 34.0$ GPa, $e_{150}^{(2)} = 4.8$ C/m^2, $\varepsilon_{110}^{(2)} = 4.64 \times 10^{-9}$ C^2/(N·m^2), $q_{150}^{(2)} = 195.0$ N/(A·m), $d_{110}^{(2)} = 0.004 \times 10^{-9}$ N·s/(V·C), $\mu_{110}^{(2)} = -201.0 \times 10^{-6}$ N·s^2/C^2, $\rho_0^{(2)} = 1000$ kg/m^3. The normalized non-homogeneity constants $\beta^{(i)}$ $(i = 1, 2)$ are varied between -2 and 2, which covers most of the practical cases. The numerical results of stress, electric displacement and magnetic flux fields are plotted in Figs.2–9. The following observations are very significant:

(i) The problem of the present paper is different from the one as shown in Refs.[7,8]. The dynamic fracture problem is studied in the present paper. However, the problems in Refs.[7,8] are all for the static anti-plane shear fracture problem. From the results, it can be shown that the singular stress, electric displacements and magnetic flux in functionally graded piezoelectric/piezomagnetic materials carry the same forms as those in homogeneous piezoelectric/piezomagnetic materials or in homogeneous piezoelectric materials but the magnitudes of intensity factors depend significantly upon the gradient of functionally graded piezoelectric/piezomagnetic material properties as discussed in Refs.[6–8].

(ii) The electro-magneto-elastic coupling effects can be obtained as shown in Eqs.(40)–(45). For electric displacement and magnetic flux intensity factors, they have the same changing tendency as the stress intensity factor as shown in Figs.2–4. However, the amplitude values of electric displacement filed, magnetic flux field and stress field are different. The amplitude values of electric displacement and magnetic flux fields are very small as shown in Figs.3 and 4. The results of electric displacement and magnetic flux intensity factors of the other cases have been omitted in the present paper.

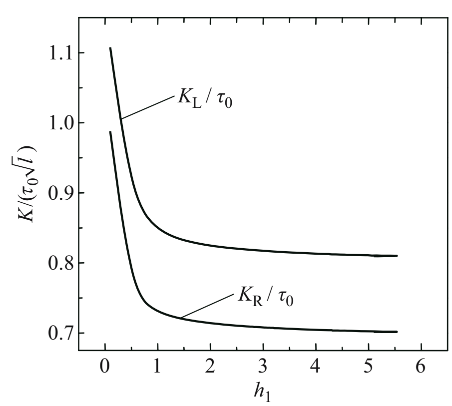

Fig.2 The stress intensity factor versus h_1 for $\beta^{(1)} = 0.3$, $b = 0.1$, $h_2 = 8.0$, $\beta^{(2)} = 0.4$ and $\omega/c_1 = 0.3$ (Material-I/Material-II)

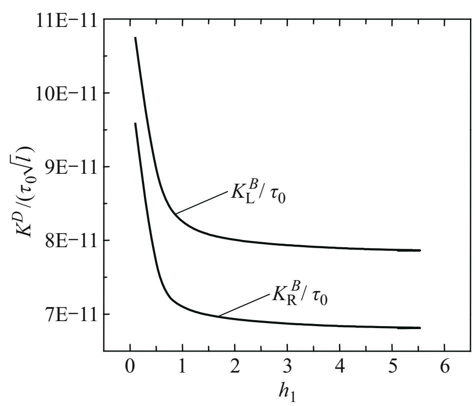

Fig.3 The electric displacement intensity factor versus h_1 for $\beta^{(1)} = 0.3$, $b = 0.1$, $h_2 = 8.0$, $\beta^{(2)} = 0.4$ and $\omega/c_1 = 0.3$ (Material-I/Material-II)

(iii) The stress intensity factors tend to decrease with the increase of the thickness of the functionally graded piezoelectric/piezomagnetic material layers, and then they tend to constants for the different cases, respectively. These constants are equal to the stress intensity factors of the interface cracks in infinite functionally graded piezoelectric/piezomagnetic material plane for the different compositive cases. From the results, it can be also concluded that the thickness effects on stress, electric displacement and magnetic flux fields near crack tips will be very small for $h_i > 4.0 (i = 1, 2)$ as shown in Figs.2–5.

(iv) From results as shown in Fig.6, the stress fields near crack tips increase with the increase of the circular frequency of the incident waves until reaching a peak value at $\omega/c_1 \approx 0.65$, then they decrease with the increase of the circular frequency of incident waves in magnitude until $\omega/c_1 \approx 1.25$. For $\omega/c_1 > 1.25$, they increase again with circular frequency of incident waves until reaching the second peak value at $\omega/c_1 \approx 1.7$, then they decrease in magnitude. The second peak value is larger than the first peak value. This phenomenon may be caused by the free boundary of the layers.

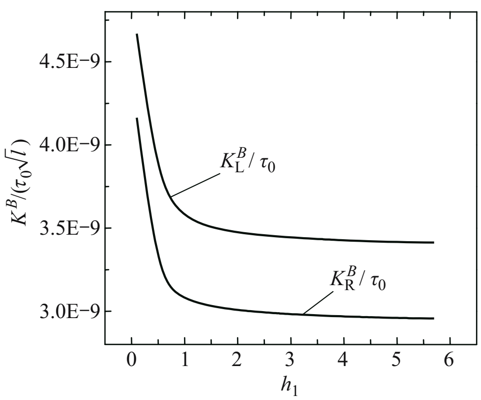

Fig.4 The magnetic flux intensity factor versus h_1 for $\beta^{(1)} = 0.3$, $b = 0.1$, $h_2 = 8.0$, $\beta^{(2)} = 0.4$ and $\omega/c_1 = 0.3$ (Material-I/Material-II)

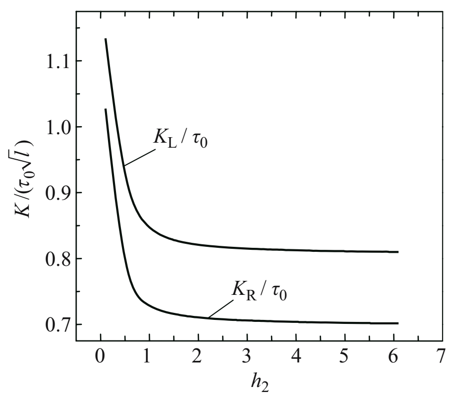

Fig.5 The stress intensity factor versus h_2 for $\beta^{(1)} = 0.3$, $b = 0.1$, $h_1 = 6.0$, $\beta^{(2)} = 0.4$ and $\omega/c_1 = 0.3$ (Material-I/Material-II)

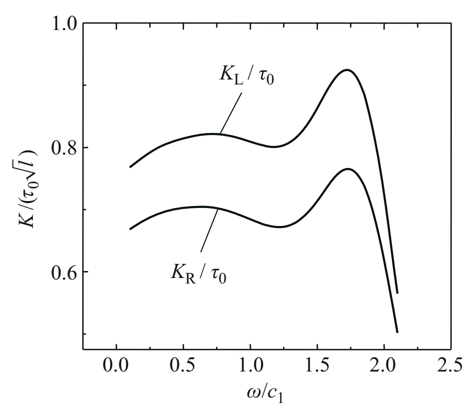

Fig.6 The stress intensity factor versus ω/c_1 for $\beta^{(1)} = 0.3$, $b = 0.1$, $h_1 = 2.0$, $\beta^{(2)} = 0.4$ and $h_2 = 8.0$ (Material-I/Material-II)

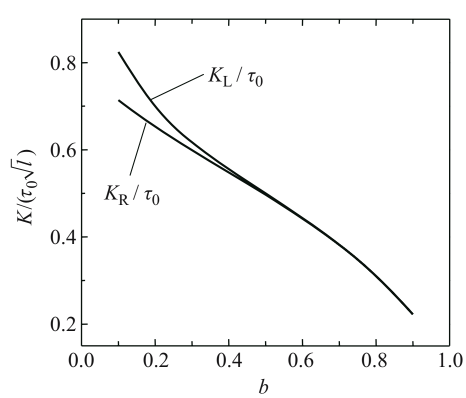

Fig.7 The stress intensity factor versus b for $\beta^{(1)} = 0.3$, $h_1 = 2.0$, $h_2 = 8.0$, $\beta^{(2)} = 0.4$ and $\omega/c_1 = 0.3$ (Material-I/Material-II)

(v) The stress fields near the inner crack tips are larger than ones at the outer crack tips as shown in Fig.8. From results as shown in Fig.7, the stress fields at crack tips decrease with the increase of the distance between two collinear cracks, i.e., the interaction of two collinear crack decreases with the increase of the distance between two collinear cracks.

(vi) The stress intensity factors tend to decrease with the increase of the functionally graded parameters $\beta^{(i)}(i=1,2)$ as shown in Figs.8–9. This means that, by adjusting the functionally graded parameters, the stress fields near crack tips can be reduced in engineering practices.

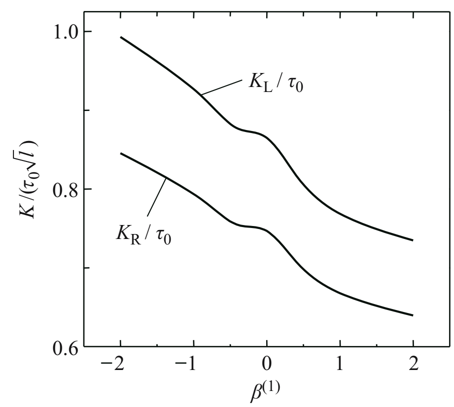

Fig.8 The stress intensity factor versus $\beta^{(1)}$ for $b=0.1$, $h_1=2.0$, $h_2=8.0$, $\beta^{(2)}=0.4$ and $\omega/c_1=0.3$ (Material-I/Material-II)

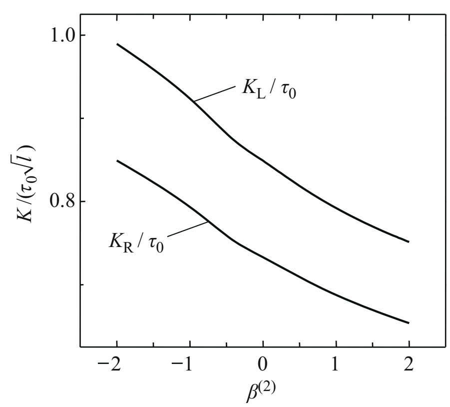

Fig.9 The stress intensity factor versus $\beta^{(2)}$ for $b=0.1$, $h_1=2.0$, $h_2=8.0$, $\beta^{(1)}=0.3$ and $\omega/c_1=0.3$ (Material-I/Material-II)

References

[1] Sih G C, Song Z F. Magnetic and electric poling effects associated with crack growth in $BaTiO_3$-$CoFe_2O_4$ composite[J]. *Theoretical and Applied Fracture Mechanics*, 2003, **39**(2):209–227.

[2] Gao C F, Tong P, Zhang T Y. Interfacial crack problems in magneto-electroelastic solids[J]. *International Journal of Engineering Science*, 2003, **41**(18):2105–2121.

[3] Liu J X, Liu X L, Zhao Y B. Green's functions for anisotropic magnetoelectroelastic solids with an elliptical cavity or a crack[J]. *International Journal of Engineering Science*, 2001, **39**(12):1405–1418.

[4] Jin D R. Functionally graded PZT/ZnO piezoelectric composites[J]. *Journal of Materials Science Letters*, 2003, **22**(5):971–974.

[5] Chen J, Liu Z X, Zou Z Z. Electriomechanical impact of a crack in functionally graded piezoelectric medium[J]. *Theoretical and Applied Fracture Mechanics*, 2003, **39**(1):47–60.

[6] Li C Y, Weng G J. Antiplane crack problem in functionally graded piezoelectric materials[J]. *Journal of Applied Mechanics*, 2002, **69**(4):481–488.

[7] Zhou Zhengong, Wang Biao. Two parallel symmetry permeable cracks in functionally graded piezoelectric/piezomagnetic materials under anti-plane shear loading[J]. *International Journal of Solids and Structures*, 2004, **41**(9):4407–4422.

[8] Zhou Zhengong, Wu Linzhi, Wang Biao. The behavior of a crack in functionally graded piezoelectric/piezomagnetic materials under anti-plane shear loading[J]. *Archive of Applied Mechanics*, 2005, **74**(8):526–535.

[9] Morse P M, Feshbach H. Methods of theoretical physics[M]. Vol.1, New York: McGraw-Hill, 1958.

[10] Soh A K, Fang D N, Lee K L. Analysis of a bi-piezoelectric ceramic layer with an interfacial crack subjected to anti-plane shear and in-plane electric loading[J]. *European Journal of Mechanics, A/Solid*, 2000, **19**(7):961–977.

[11] Ozturk M, Erdogan F. Mode I crack problem in an inhomogeneous orthotropic medium[J]. *International Journal of Engineering Science*, 1997, **35**(3):869–883.

[12] Gradshteyn I S, Ryzhik I M. Table of integral, series and products[M]. New York: Academic Press, 1980.

[13] Erdelyi A. Tables of integral transforms[M]. Vol.1, New York: McGraw-Hill, 1954.

[14] Zhou Zhengong, Wang Biao. The dynamic behavior of two parallel symmetry cracks in magneto-electro-elastic composites under harmonic anti-plane shear waves[J]. *Applied Mathematics and Mechanics*(*English Eidtion*), 2006, **27**(5):583–591.

[15] Zhou Zhengong, Wang Biao. Scattering of harmonic anti-plane shear waves by an interface crack in magneto-electro-elastic composites[J]. *Applied Mathematics and Mechanics* (*English Edition*), 2005, **26**(1):17–26.

[16] Zhou Zhengong, Wang Biao. Investigation of the behavior of a mode-I interface crack in piezoelectric materials by using the Schmidt method[J]. *Applied Mathematics and Mechanics* (*English Edition*), 2006, **27**(7):871–882.

[17] Li Lin, Zhou Zhengong, Wang Biao. Scattering of anti-plane shear waves in functionally graded material strip with an off-center vertical crack[J]. *Applied Mathematics and Mechanics* (*English Edition*), 2006, **26**(6):731–740.